A physical model for liquid movement into a porous substrate under the action of a pressure pulse

Li Yang

KEYWORDS: Printing dynamics, Nip-pressure profile, Ink dynamics, Ink-transfer.

SUMMARY: The dynamic behavior of ink movement under nip-pressure of a printing press has been studied. The theoretical model employed originates from the Bosanquet model that was previously applied to situations of constant or zero external pressures. In the present work, we extend the model to a printing situation where a time-dependent nip pressure presents. The general solution of the model for a simple liquid has been worked out, as in most situations the ink's continuous phase can be approached as a Newtonian fluid, e.g. mineral oil in offset and water in flexo etc. The general solution is of analytical form thanks to the possibility to expand the nip-pressure profile into a Fourier series. For illustrative purposes, simulations with three model profiles, one rectangular, one sinusoidal, and one joint sinusoidal, have been performed. It is found that the profile of the nip-pressure plays a dominant role in liquid transfer and setting.

ADDRESs OF THE AUTHOR: Li Yang (li.yang@innventia.com), Innventia AB, Drottning Kristinas väg 61, 11486 Stockholm, Sweden

In conventional printing technologies, for instance offset and flexography, ink-transfer is achieved by direct nip-paper contact with pressure. The contact time is typically a few milliseconds (ms), depending on the printing speed and the width of the nip-paper contact.

Ink dynamics and ink-transfer are complicated. Despite extensive studies reported in literature, there are still things which remain unknown. Concerning the effects of ink, the major ink-properties identified are viscosity, surface tension, ink-tack, etc. In parallel, there are also many investigations conducted concerning the effects of paper properties, using both model and commercial paper substrates. The major paper properties are porosity and pore distribution, permeability, surface energy, surface roughness, etc. When it comes to ink-paper interaction, contact angle is one of the most important parameters. In addition to the material properties, printing parameters are known to be important, such as line nip pressure, printing speed, and so on. Nevertheless, one has to bear in mind that not all of these parameters or properties are equally important under all circumstances. Therefore, an application of the accumulated knowledge is not straightforward.

Understanding of ink dynamics and ink transfer requires reliable physical model to bring light to the experimental observations. Even though there has been a lot of knowledge generated and accumulated, most of the knowledge is qualitative. Due to the complexity of the ink dynamics, it is nearly impossible to isolate the contribution of one parameter from other parameters by experimental means. For example reducing surface roughness by calendering affects even pore structure of the paper. On the other hand, the investigation would be very costly, even if it was technically possible. On the contrary, these are rather easy to be achieved with the help of modeling and simulation. Eventually, it is possible to investigate the effects of each of the relevant parameters on the ink dynamics, at will, such as ink tack, compression duration, etc. This provides one with detailed insights into ink dynamics. Moreover, modeling and simulation are both time and cost effective ways of investigation.

There are a few models proposed, based either on experiences (empirical) or on the first principle. Lucas-Washburn (L-W) model (Washburn, 1921) is a simple and popular model employed frequently for studying capillary-driven processes. According to the L-W model, a substrate with big pores absorbs a liquid faster and the distance of the liquid flow increases with the square-root of time,

$$x = \sqrt{\frac{R\gamma\cos\theta}{2\eta}\,t} \propto (Rt)^{1/2} \qquad [1]$$

where R is the radius of the pore, η and γ are the viscosity and the surface tension of the liquid, and θ the contact angle.

The Bosanquet (1923) model is an extension of the L-W model, which had also been used for studying capillary-driven processes. Compared to the L-W model, forces due to exchanges of the momentum of the liquid column are included in the Bosanquet model, provided that the Poiseuille's law applies. Bosanquet studied the effects of the force due to momentum exchange of ink fluid in a capillary tube and the circumstances under which these effects become inappreciable. *Eq 2* is the mathematical form of the Bosanquet model,

$$\frac{d}{dt}\left(\pi R^2\rho x\frac{dx}{dt}\right) + 8\pi\eta x\frac{dx}{dt} = P_e\pi R^2 + 2\pi R\gamma\cos\theta \qquad [2]$$

The first term on the left-hand side is the force due to the momentum exchange of the liquid in a capillary tube of radius, R. The quantities ρ and x are the mass density and the length of the fluid column. The second term is the viscosity drag of the liquid. On the right-hand side, the first term originates from the external pressure, P_e, that was treated as constant. And the second term corresponds to the capillary force.

Eq 2 can be written in a more compact form,

$$\frac{d}{dt}(xx') + axx' = b \qquad [3]$$

where x' is the time-derivative of x and a and b are constants defined as

$$a = \frac{8\eta}{R^2\rho}, \qquad b = \frac{P_e}{\rho} + \frac{2\gamma\cos\theta}{R\rho}. \qquad [4]$$

The solution presented in the literatures (Bosanquet 1923; Schoelkopf et al 2000), is

$$x^2 = \frac{2b}{a^2}\exp(-at) + \frac{2b}{a}t - \frac{2b}{a^2}. \quad [5]$$

In contradiction to the L-W predictions, shown in *Eq 1*, there is plentiful experimental evidence showing that liquid sets faster into a substrate with smaller pores than that with big pores, provided identical porosities of these substrates. To understand this, Schoelkopf et al (2000) conducted simulations, incorporating the Bosanquet model with the Pore-Cor unit cell (Matthews et al 1993) simulation techniques. In the simulations, the external force was ignored (P_e=0). They found that for a liquid of low viscosity and at the very beginning of the liquid penetration, so that $\frac{8\eta}{R^2\rho}t << 1$, the distance of the liquid flow is given by,

$$x = \sqrt{\frac{2\gamma\cos\theta}{R\rho}t} \propto \frac{t}{\sqrt{R}} \quad [6]$$

Schoelkopf et al referred to the regime that follows *Eq 6* "inertial flow". Compared to the capillary flow characteristics described in *Eq 1*, the inertia flow differs in the following ways. First, the distance of the liquid flow increases linearly with time. Hence the singularity of L-W model at t=0, having infinite ink velocity, does no longer exist. Second, the distance of the liquid flow is inversely proportional to the square root of the radius of the pore and the fluid density, implying that the liquid initially moves faster in smaller pores. Based on the simulation results, they concluded that there are two regimes, an inertia flow and a capillary flow. As time goes on, the liquid's movement transfers from inertia flow to capillary flow.

Xiang and Bousfield (2000) also observed that a substrate with smaller pores sets ink faster than that with large pores, which contradicted the L-W model. They argued that while ink sets its solid particles may form a filtercake on the substrate's surface and the filtercake controls the absorption rate into the porous substrate. Based on the Darcy law, they put forward the filtercake model. In this model, the distance of ink flow is expressed as

$$x = \sqrt{\frac{R\gamma t\cos\theta}{2\eta\left(1 + \frac{\varepsilon\varphi_s R^2}{8K\varphi_f(1-\varphi_s)}\right)}} \quad [7]$$

In this expression, ε is the void fraction in the coating layer; φ_s and φ_f are the volume fractions of solid ink and solid in the filter cake. The quantity K is the Darcy coefficient of the filter cake, which is responsible for the effect of the filter cake.

Rioux (2003) studied the short time absorption rate driven by capillary force on seven uncoated and eleven coater papers. The absorption rate was measured with a Bristow Wheel device, which was complemented with gloss dynamics measurement of freshly printed samples and tack dynamics measurement. The predictions with the L-W model were partly confirmed by the experimental observations.

The behavior of ink dynamics under printing nip is not well understood. The short time duration in combination with drastic time-dependence of the nip-pressure makes an experimental study very difficult. On the theoretical side, there have been a couple of studies performed in recent years. Dubé et al (2008) simulated the ink-transfer process by numerical simulation based on the Navier-Stokes equation. The nip pressures adapted in the simulation correspond to a flat plat that moves vertically to (positive pressure) or away from (negative pressure) the paper substrate. The numerical simulation was followed up and further improved by Holmvall et al (2011), who introduced the immersed and moving boundary method into the simulation.

The objective of this work is to extend the application of the Bosanquet model to a printing situation, where an arbitrary and time-dependent nip-pressure presents.

Bosanquet model for a printing situation

The differential equation and the general solution

The Bosanquet model applies for a simple liquid as in most situations the ink's continuous phase can be approached as a Newtonian fluid, e.g. mineral oil in offset and water in flexography etc. When applied to a printing situation, like offset and flexography, the external pressure in *Eq 2* comes from the printing nip, which is usually a short time pulse of strong time-dependence. To distinguish from the solutions previously reported in the literatures that correspond to the case of zero or constant (time-independent) pressure, the external pressure is explicitly written as $P_e(t)$. Consequently, the quantity b defined in *Eq 4* also becomes time-dependent,

$$b(t) = \frac{P_e(t)}{\rho} + \frac{2\gamma\cos\theta}{R\rho} \quad [8]$$

Therefore, when applied to a printing situation, the corresponding expression to *Eq 3* becomes,

$$\frac{d}{dt}(xx') + axx' = b(t). \quad [9]$$

One can prove that the general solution of *Eq 9* is

$$\begin{aligned} xx' &= \exp(-at)\left(\int \exp(at)b(t)dt + C\right) \\ &= C\exp(-at) + \exp(-at)\int \exp(at)\frac{P_e(t)}{\rho}dt + \frac{2\gamma\cos\theta}{aR\rho} \end{aligned} \quad [10]$$

where C is an integrating constant. From *Eq 10* one can further obtain,

$$\begin{aligned} x^2 = &-\frac{2C}{a}\exp(-at) + \frac{2}{\rho}\int\left[\exp(-at)\left(\int \exp(at)P_e(t)dt\right)\right]dt \\ &+ \frac{R\gamma\cos\theta}{2\eta}t + D \end{aligned} \quad [11]$$

Similar to C, D is another integrating constant. The details of how these quantities, C and D, are determined from initial conditions are presented in the Appendix, using sinusoidal nip profile as an example. Be aware of that the integrating constants are nip-profiles related, as also indicated in the Appendix.

In *Eq 11*, the first term on the right hand side originates from the inertial movement of the liquid, which decreases exponentially with time because of increased viscosity drag. As seen in *Eq 2* the viscosity drag increases linearly with speed, which quickly balances the external force and/or capillary drag. As the consequence, the acceleration of the liquid movement decreases. Hence

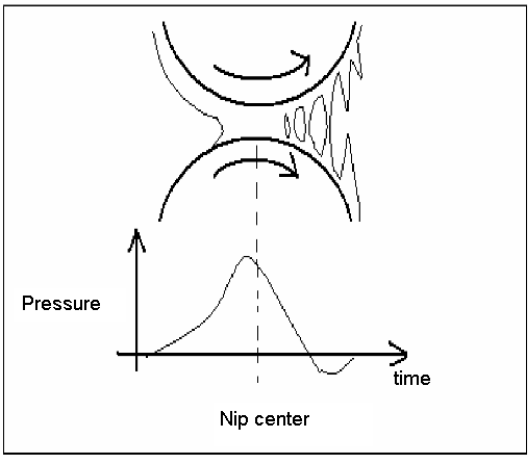

Fig 1. The printing nip and pressure pulse (Bäckström, 2004).

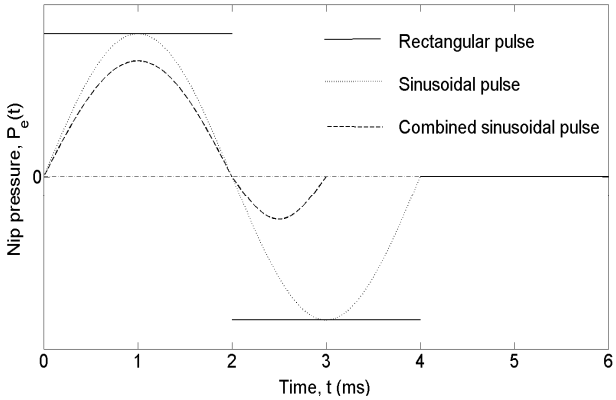

Fig 2. Nip-pressure profiles used in simulations. The positive nip-pressure corresponds to the compressing regime while the negative nip-pressure to the ink-splitting regime.

this term contributes only at the very beginning of the liquid-transfer process. The second term is from the external pressure exerted by the printing nip. It is obvious that the expression for x varies with the profile of the nip-pressure and this term vanishes when the nip-pressure pulse ends. The third term is because of the capillary force. The short-time nature of the first two terms justifies the validity of the L-W model when studying the long-term trend of liquid imbibitions.

Eq 11 is the principal result of the present work, which is also the general solution of the Bosanquet model (*Eq 9*) when applied to a printing situation with any time-dependent nip-profile. The solution worked out by Bosanquet (1923) and Schoelkopf et al (2000) is only a special case of the present solution, corresponding to a constant external pressure ($P_e(t)$=const.). The explicit expression for x^2 varies with the mathematical form of time-dependent pressure profile. As an example, the solution corresponding to the sinusoidal nip profile is given in the Appendix.

In *Eq 11*, it has been assumed that $\gamma cos\theta$ remains unchanged over the time under the nip-pressure, which is probably not true. Nevertheless, the nip-pressure is much stronger than the capillary pressure and the impact of such a simplification is limited.

Even though the Bosanquet model eliminates the problem of infinite velocity at t=0, existing in the L-W model, there is still a drawback associate with this approach because the solution to *Eq 2* is undefined either at t=0 as being pointed out by Ridgway et al (2002a,b). The authors also suggested two methods to practically overcome this drawback, which give indistinguishable results according to their simulations. One of the methods is to apply boundary conditions as limits on the velocity and position which approach zero but do not actually start from zero.

Model profiles of nip-pressure

The nip-paper interaction may be subdivided into three regimes: compression, decompression, and (ink filament) splitting. The nip-pressure changes dramatically in the due course. *Fig 1* highlights the time variation of the nip-pressure. The nip pressure increases along time in the compression regime when the paper approaches the center of the nip. After passing through the narrowest gap between the nip-cylinders, the nip pressure decreases with time (decompression). At the exiting point of the press nip, the nip pressure totally vanishes (zero pressure). Even though there is no longer nip compression after the exiting point, the nip-paper interaction continues for a short while in the ink-splitting regime. Connected by ink filaments the nip exerts instead a negative pressure to the ink transferred onto the paper surface. According to literatures (Dubè et al, 2008), the negative nip pressure depends on the extensional viscosity and the surface tension of the ink, the radius and the number of ink filaments, the separating speed of the nip-cylinders (or the speed of ink-splitting) etc.

Nip pressure has a predominant effect on ink transfer. The effect may differ significantly between print on coated grades from that on uncoated grades. As an uncoated paper often comprises surface and internal pores of big sizes, all of the ink components may be pressed into the paper structure by the nip. While for coated substrate, due to smaller pore size on the paper surface, only the ink-vehicles can be pressed into the pore structure provided that pigment ink is used. This qualitatively explains the differences in ink-penetration and print through for prints on uncoated and coated grades.

An ink penetration into the paper structure may cause severe print quality problems. It results not only in reduced optical density or reduced color saturation (Yang et al. 2005a,2005b), but also print-through, making the print visible from the reverse side of the print (Pauler 1987; Bristow 1988).

Simulations and examples

In this section, we will demonstrate how to apply *Eq 11* to study the ink dynamics governed by the effective nip-pressure, $P_e(t)$. The presented method is universal, but for illustrative purpose, the following parameters which may be representative for offset print on newsprint grade are used in the simulation. They are the peak nip-pressure, P_0=10^7 Pa; viscosity, η=1 Pas; pore radius, R=1μm; nip width, L=40 mm; press speed V=10 m/s; ink density, ρ=10^3 kg/m^3; contact angle, θ=30^o; surface energy, γ=0.1 N/m. The time duration of the nip pulse equals then T=L/V=4ms. Assuming a constant contact angle is obviously a simplification to reality when nip-pressure

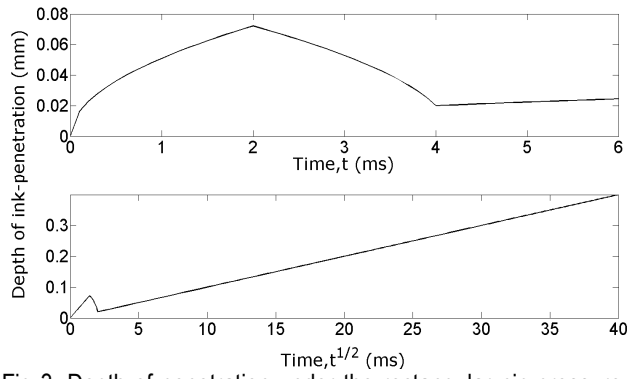

Fig 3. Depth of penetration under the rectangular nip-pressure pulse.

presents. Nevertheless as the nip-pressure is much stronger than the capillary force, such a simplification has rather limited effect on the simulated results.

The nip-paper interaction consists of three distinct regimes, compression, decompression, and detaching (film-splitting). In the compression and decompression regimes, the nip exerts a positive pressure, pushing ink or ink vehicle into the paper pore structure. On the contrary, when the printing nip detaches from the paper, ink filaments built up. When moving away from the paper, the nip pulls the ink filaments, which becomes a negative pressure to the ink that connects the paper substrate.

Fig 2 illustrates three profiles of the nip pressures. The rectangular form represents the situation with two big nip-cylinders between which the gap is nearly constant. This profile is obviously a rough approximation to the real process. The single sinusoidal pulse profile (dotted line) takes the variation of the gap between the nip cylinders into consideration, when paper approaches and exits the center of the nips. This profile is symmetric in compression and slitting forces. Comparing with dynamic characteristics under the rectangular pulse, one can study the influence of the nip-profiles (shapes) on the ink dynamics. The third nip-profile joints pieces of two sinusoidal profiles (dot-dashed line). This is designed to investigate the effect of non-symmetric compression and splitting profile on the ink dynamics and the ink transfer. It is evident that this profile is an even better approximation to the reality. By setting the second piece as zero, one can study inks of little extensional viscosity (zero tack).

In addition to these model profiles, possibilities to extend the present approach to an arbitrary nip profile are also presented.

The rectangular pressure pulse

Eq 12 is the mathematical expression for the nip-profile, which is comprised of three time regimes, namely

$$P_e(t)=\begin{cases} P_0, & (t\le\frac{T}{2}) \\ -P_0, & (\frac{T}{2}<t\le T) \\ 0, & (t>T) \end{cases} \qquad [12]$$

where T stands for the time duration of ink-nip contact. In this profile, the regime with positive nip pressure corresponds to the compression and decompression processes while the negative nip pressure to the splitting process due to ink-tack. This is obviously a very rough approximation to the real nip-contact.

Fig 3 depicts the dynamic characteristics of ink penetration, when a rectangular nip pressure is applied. Naturally, with a positive nip-pressure, the depth of ink-penetration increases with time. After reaching the maximum depth at the end of the compression & decompression processes (t=T/2=2ms), the depth declines with time because of negative nip-pressure originated from the ink-tack. Despite the same amplitude and time duration of the negative nip pressure as those of the positive, the depth of ink-penetration does not return to zero when the nip pulse ends at t=T=4ms. This is because of the presence of capillary force that holds a portion of the ink inside the pore. For convenience of further discussion, we called it residual depth hereafter. After the nip, the movement of the ink is solely governed by a capillary force. In the capillary regime, the depth of ink penetration is proportional to the square-root of time as shown in the lower half in *Fig 3*, as long as there is ink remaining on the paper surface.

The present model can be applied to substrate with several pores in a straightforward fashion. For a collection of identical pores, it is obvious that, at constant porosity, the amount of fluid transferred to the substrate is larger when the pores are smaller. This is because the smaller pores are more efficient at retaining the fluid when the nip cylinder recedes from the substrate. This is in line with the predications based on the Navier-Stokes equations (Bubé et al 2008).

The sinusoidal nip-pressure pulse

The mathematical expression for the sinusoidal nip pressure (dotted line in Fig. 2) is,

$$P_e(t)=\begin{cases} P_0\sin(\frac{2\pi}{T}t)=P_0\,\mathrm{Im}\left[\exp\left(i\frac{2\pi}{T}t\right)\right], & (0<t\le T) \\ 0, & (t>T) \end{cases} \qquad [13]$$

This is obviously a better approximation compared to the rectangular one. In the compression & decompression regimes, the nip-pressure increases when paper approaches the center of compression and then decreases after that. The explicit solution has been worked out and shown in the Appendix, which gives

$$x^2=\begin{cases} -\frac{2C_1}{a}\exp(-at)-\frac{2P_0}{\rho\left(a^2+\frac{4\pi^2}{T^2}\right)}\left\{\frac{aT}{2\pi}\cos\left(\frac{2\pi}{T}t\right)+\sin\left(\frac{2\pi}{T}t\right)\right\}+\frac{4\gamma\cos\theta}{aR\rho}t+D_1, & (t\le T) \\ -\frac{2C_2}{a}\exp(-at)+\frac{4\gamma\cos\theta}{aR\rho}t+D_2, & (t>T) \end{cases} \qquad [14]$$

where

$$C_1 = \frac{2\pi P_0}{\rho T\left(a^2 + \frac{4\pi^2}{T^2}\right)} - \frac{2\gamma\cos\theta}{aR\rho},$$

$$D_1 = \frac{2C_1}{a} + \frac{P_0 aT}{\rho\pi\left(a^2 + \frac{4\pi^2}{T^2}\right)}.$$

and

$$C_2\exp(-aT) = C_1\exp(-aT) - \frac{2\pi P_0}{\rho T\left(a^2 + \frac{4\pi^2}{T^2}\right)},$$

$$D_2 = \left[x^2\right]_{t=T} + \frac{2C_2}{a}\exp(-aT) - \frac{4\gamma T\cos\theta}{aR\rho}$$

with

$$\left[x^2\right]_{t=T} = -\frac{2C_1}{a}\exp(-aT) - \frac{P_0 aT}{\pi\rho\left(a^2 + \frac{4\pi^2}{T^2}\right)} + \frac{4\gamma\cos\theta}{aR\rho}T + D_1$$

Fig 4 shows the liquid movement under the nip-pressure, which is in large similar to that under the rectangular nip-pressure, even though the maximum depth (at t=T/2=2ms) reached by the ink is less deep. Moreover the residual depth of ink-penetration at the end of the nip contact (t=T=4ms) is nearly the same as with the rectangular nip-pressure. These indicate that the major characteristics of the ink dynamics can still be captured even with a rough approximation like the rectangular one. In other words, the amplitude and the duration of the nip pulse are the most important while the exact shape of the nip pulse comes to a second place.

The jointed sinusoidal nip-pressure pulse

Even though the sinusoidal profile approximates better the reality in the compression regime, it is still too rough in the ink-splitting regime. The ink-splitting regime is usually lower in amplitude and shorter in duration time, as suggested by *Fig 1*. To better reflect the reality, we proposed another nip-pressure profile that joints two separate sinusoidal pieces as the following:

$$P_e(t) = \begin{cases} P_1\sin\left(\frac{2\pi}{T_1}t\right), & \left(0 < t \le \frac{T_1}{2}\right) \\ P_2\sin\left(\frac{2\pi}{T_2}\left(t - \frac{T_1}{2}\right) + \pi\right), & \left(\frac{T_1}{2} < t \le \frac{T_1+T_2}{2}\right) \\ 0, & \left(t > \frac{T_1+T_2}{2}\right) \end{cases} \quad [15]$$

In this profile, P_1 and T_1 are the characteristic parameters of the compression & decompression regimes. Their values depends on the line-load of the press (or distance between the nip-cylinders), the printing speed, and the radius and compressibility of the nip-cylinder and the paper. P_2 and T_2 are the characteristic parameters of ink-splitting process, which depend mainly on the ink-properties, such as extensional viscosity and ink tack, absorbency of the paper and to some extend the nip-properties as well.

Fig 5 shows the ink dynamics under this nip profile. As seen in the ink-splitting regime, the ink-penetration depth reduces only slightly due to reduced amplitude of the negative nip pressure and shorter interaction time (T_2)

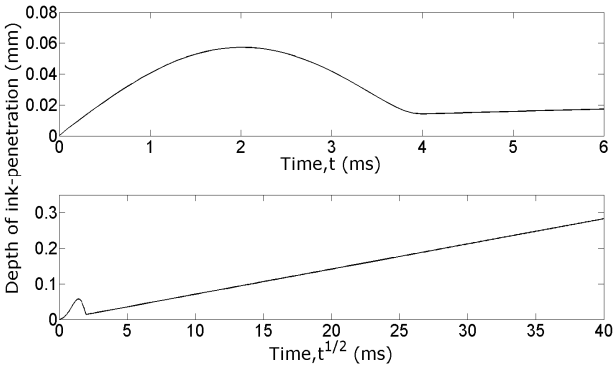

Fig 4. Depth of penetration under the sinusoidal nip-pressure pulse.

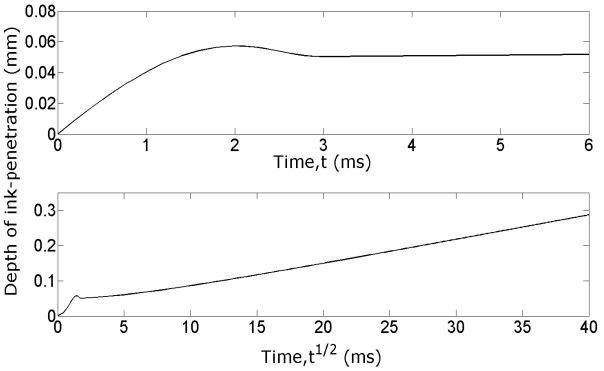

Fig 5. Depth of penetration under the jointed sinusoidal nip-pressure pulse. All the parameters are the same as in the proceeding simulations except for P_2= P_0/2 and T_2=T/2.

compared to the case of sinusoidal profile. This reveals the importance of ink properties on ink-penetration, especially the extensional viscosity or the ink-tack. In other words, ink dynamics may significantly be modified by manipulation of ink properties. The time dependence of ink-penetration in the capillary regime deviates significantly from the $t^{1/2}$ characteristics. This can be attributed to the large residual-depth at t=(T_1+T_2)/2 when the nip-pressure ends.

Extension to an arbitrary nip profile

In practice, a true nip profile often deviates from a perfect sinusoidal form. This deviation may be regarded as contributions from higher order of harmonics or the true profile which can possibly be expressed in form of Fourier series,

$$P_e(t) = \mathrm{Im}\left\{\sum_n a_n\exp\left(in\frac{2\pi}{T}\right)\right\} \quad [16]$$

The accuracy of Fourier expansion depends on the number of expansion terms. Considering the fact that the nip pressure is sinusoidal-alike, one may expect that the Fourier expansion would be sufficiently accurate to include only a few terms.

It is obvious that the integral involving $P_e(t)$ in Eq 11 is analytically obtainable, as it only contains terms of the following form

$$\sum a_n\int\left[\exp\left(-\frac{8\eta}{R^2\rho}t\right)\left(\int\exp\left[\left(\frac{8\eta}{R^2\rho} + in\frac{2\pi}{T}\right)t\right]dt\right)\right]dt \quad [17]$$

Hence the analytic expression for *Eq 11* can be obtained for an arbitrary nip-profile, regardless of the number of the expansion terms.

Conclusions

The dynamics and transfer of a Newtonian liquid have been studied by incorporating the Bosanquet model with an arbitrary and time-dependent external pressure pulse. The general solution of the model has been worked out, which consists of three parts, governed by the liquid inertia, the nip-pressure pulse, and capillary pressure, respectively, which are active in different time scales. The inertia term is active only in the very beginning of the printing process, as it decreases exponentially with time. The nip-pressure term dominates ink-dynamics and ink transfer during the period of time when compression, decomposition and splitting occur. The capillary pressure takes over after the nip contact. The short-time nature of the first two terms justifies the validity of the L-W model when studying the long-term trend of liquid imbibitions. Despite only contributing in a short term, the inclusion of the inertia term is still important as it avoids the singularity (at t=o) that exists in the L-W model.

The general solution in analytic form is in principle obtainable for an arbitrary time-dependent nip profile thanks to the possibility to expand the nip profile into a Fourier series of limited expansion terms. This makes it an attractive method for quantitative and systematic evaluations of the effects of individual parameters, such as press speed, nip width, viscosity of ink, pore size of paper substrate, etc. Such evaluation will be valuable for developments of printing processes and properties of the materials (ink and paper) involved.

Simulations of dynamics and transfer behavior of the liquid have been conducted, using three types of nip-pressure profiles. It has been found that the amplitudes of compression & decomposition and splitting (negative pressure) parts of the profiles are important for the ink dynamics and ink transfer, while the exact form of the profile is relatively less important. The simulations are in line with some of the previous predictions based on the more sophisticated model, e.g. Navier-Stokes equations.

Acknowledgement

Financial supports from Research Institute of Sweden (RISE) and Hai Ju Gong Cheng (Beijing, China) are acknowledged.

Literature

Bosanquet, C.H. (1923), "On the flow of liquids into capillary tubes", Philos. Mag. 45, 525.

Bristow, J.A. (1988), "Print-through and Ink Penetration - A Mathematical Treatment", in Adv. Printing Sci. Technol. 19, Pentech. Press , 137-145 .

Bäckström, M. (2004), "Development of a method for pre-damping in laboratory offset printing units", MSc. thesis, Luleå Univ., ISSN 1402-1617, ISRN LTU-EX--04/195--SE , also available online at http://epubl.luth.se/1402-1617/2004/195/LTU-EX-04195-SE.pdf.

Dubé, M., Drolet, F., Daneault, C. and Mangin, P.J. (2008), "Hydrodynamics of fluid transfer", J. Pulp Pap. Sci. 34, 174-181.

Holmvall, M., Drolet, F., Uesaka, T. and Lindström, S. (2011), "Micro-fluidics in Printing nip liquid transfer on random fibre network surface", in Proc. Paper Phys. Seminar, 67-68, in Graz, Austria.

Matthews, G.P., Moss, A.K., Spearing, M.C. and Voland, F. (1993), ""Network calculation of mercury Intrusion and absolute permeability In sandstone and other porous media", Power Technol. 76, 95-107.

Pauler, N. (1987), "A Model for the Interaction between Ink and Paper", in Adv. Printing Sci. and Technol. 19, 116-136 (Pentech. Press).

Rioux, R.W. (2003), "The rate of fluid absorption in porous media", MSc. thesis, Univ. Maine, available online at http://www.library.umaine.edu/theses/pdf/RiouxRW2003.pdf.

Ridgway, C.J., Gane, P.A.C., Schoelkopf, J. (2002a), "Effect of capillary element aspect ratio on the dynamic imbibition with porous networks", Journal of Colloid and Interface Science 252, 373–382.

Ridgway, C.J. and Gane, P.A.C. (2002b), "Controlling the absorption dynamics of water-based ink into porous pigmented coating structures to enhance print performance", Nord. Pupl Pap. Res. J. 17, 119-129.

Schoelkopf, J., Gane, P.A.C., Ridgway, C.J. and Matthews, G.P. (2000), "Influence of inertia on liquid absorption into paper coating structures", Nord. Pulp Pap. Res. J. 15, 422-430.

Xiang, Y. and Bousfield, D.W. (2000), "Influence of coating structure on ink tack dynamics", J. Pulp Pap. Sci. 26(6), 221-227.

Washburn, E.W. (1921), "The dynamics of capillary flow", Phys. Rev. 17, 271-283.

Yang, L., Fogden, A., Pauler, N., Sävborg, Ö. and Kruse, B. (2005a), "A novel method for studying ink penetration of printing", Nord. Pupl Pap. Res. J. 20, 399-405.

Yang, L., Fogden, A., Pauler, N., Sävborg, Ö and Kruse, B (2005b), "Studying Ink Penetration with Microscopic and Spectroscopic Techniques", J. Imaging Sci. Technol. 50, 327-332.

Manuscript received May 24, 2012
Accepted December 20, 2012

Appendix: Solution of printing with the sinusoidal nip-pressure pulse

The mathematical expression for the sinusoidal nip profile is

$$P_e(t) = \begin{cases} P_0 \sin(\frac{2\pi}{T}t), & (0 < t \le T) \\ 0, & (t > T) \end{cases} \qquad [A1]$$

It is easier to use the exponential form of the sinus, namely

$$\sin\left(\frac{2\pi}{T}t\right) = \mathrm{Im}\left[\exp\left(i\frac{2\pi}{T}t\right)\right] \qquad [A2]$$

Then the integration in *Eq 11* can readily be worked out as following

$$\int \exp(at)\frac{P_e(t)}{\rho}dt = \frac{P_0}{\rho}\,\mathrm{Im}\left\{\int \exp\left(at + i\frac{2\pi}{T}t\right)dt\right\}$$
$$= \frac{P_0}{\rho}\,\mathrm{Im}\left\{\frac{1}{a + i\frac{2\pi}{T}}\exp\left(at + i\frac{2\pi}{T}t\right)\right\} \qquad [A3]$$
$$= \frac{P_0}{\rho\left(a^2 + \frac{4\pi^2}{T^2}\right)}\exp(at)\left\{a\sin\left(\frac{2\pi}{T}t\right) - \frac{2\pi}{T}\cos\left(\frac{2\pi}{T}t\right)\right\}$$

Consequently, the integral in *Eq 11* is simplified as

$$\int\left[\exp(-at)\left(\int \exp(at)\frac{P_e(t)}{\rho}dt\right)\right]dt = \frac{P_0}{\rho\left(a^2 + \frac{4\pi^2}{T^2}\right)}\int\left\{a\sin\left(\frac{2\pi}{T}t\right) - \frac{2\pi}{T}\cos\left(\frac{2\pi}{T}t\right)\right\}dt \qquad [A4]$$
$$= \frac{-P_0}{\rho\left(a^2 + \frac{4\pi^2}{T^2}\right)}\left\{\frac{aT}{2\pi}\cos\left(\frac{2\pi}{T}t\right) + \sin\left(\frac{2\pi}{T}t\right)\right\}$$

Hence one receives,
$$xx' = \begin{cases} C_1\exp(-at) + \dfrac{P_0\left[a\sin\left(\frac{2\pi}{T}t\right) - \frac{2\pi}{T}\cos\left(\frac{2\pi}{T}t\right)\right]}{\rho\left(a^2 + \frac{4\pi^2}{T^2}\right)} + \dfrac{2\gamma\cos\theta}{aR\rho}, & (t \le T) \\ C_2\exp(-at) + \dfrac{2\gamma\cos\theta}{aR\rho}, & (t > T) \end{cases} \qquad [A5]$$

and
$$x^2 = \begin{cases} -\dfrac{2C_1}{a}\exp(-at) - \dfrac{2P_0}{\rho\left(a^2 + \frac{4\pi^2}{T^2}\right)}\left\{\dfrac{aT}{2\pi}\cos\left(\frac{2\pi}{T}t\right) + \sin\left(\frac{2\pi}{T}t\right)\right\} + \dfrac{4\gamma\cos\theta}{aR\rho}t + D_1, & (t \le T) \\ -\dfrac{2C_2}{a}\exp(-at) + \dfrac{4\gamma\cos\theta}{aR\rho}t + D_2, & (t > T) \end{cases} \qquad [A6]$$

By applying the initial conditions, at t=0,
$$[xx']_{t=0} = 0, \qquad [A7]$$
$$[x^2]_{t=0} = 0,$$

one obtains,
$$C_1 = \frac{2\pi P_0}{\rho T\left(a^2 + \frac{4\pi^2}{T^2}\right)} - \frac{2\gamma\cos\theta}{aR\rho}, \qquad [A8]$$
$$D_1 = \frac{2C_1}{a} + \frac{P_0 aT}{\rho\pi\left(a^2 + \frac{4\pi^2}{T^2}\right)}.$$

Similarly, employing the continuity conditions at t=T, one receives the relationships given in *Eqs A9* and *A10* from which the quantities, C_2 and D_2, can be determined.

$$C_2\exp(-aT) = C_1\exp(-aT) - \frac{2\pi P_0}{\rho T\left(a^2 + \frac{4\pi^2}{T^2}\right)}, \qquad [A9]$$
$$D_2 = [x^2]_{t=T} + \frac{2C_2}{a}\exp(-aT) - \frac{4\gamma T\cos\theta}{aR\rho}$$

with
$$[x^2]_{t=T} = -\frac{2C_1}{a}\exp(-aT) - \frac{P_0 aT}{\pi\rho\left(a^2 + \frac{4\pi^2}{T^2}\right)} + \frac{4\gamma\cos\theta}{aR\rho}T + D_1 \qquad [A10]$$